BRAIN COMMUNICATIONS

Cerebral atrophy in amyotrophic lateral sclerosis parallels the pathological distribution of TDP43

Mahsa Dadar,[1] Ana Laura Manera,[1] Lorne Zinman,[2] Lawrence Korngut,[3,4,5] Angela Genge,[6] Simon J. Graham,[2] Richard Frayne,[3,4,5] D. Louis Collins[1] and Sanjay Kalra[7,8]

Amyotrophic lateral sclerosis is a neurodegenerative disease characterized by a preferential involvement of both upper and lower motor neurons. Evidence from neuroimaging and post-mortem studies confirms additional involvement of brain regions extending beyond the motor cortex. The aim of this study was to assess the extent of cerebral disease in amyotrophic lateral sclerosis cross-sectionally and longitudinally and to compare the findings with a recently proposed disease-staging model of amyotrophic lateral sclerosis pathology. Deformation-based morphometry was used to identify the patterns of brain atrophy associated with amyotrophic lateral sclerosis and to assess their relationship with clinical symptoms. Longitudinal T_1-weighted MRI data and clinical measures were acquired at baseline, 4 months and 8 months, from 66 patients and 43 age-matched controls who participated in the Canadian Amyotrophic Lateral Sclerosis Neuroimaging Consortium study. Whole brain voxel-wise mixed-effects modelling analysis showed extensive atrophy patterns differentiating patients from the normal controls. Cerebral atrophy was present in the motor cortex and corticospinal tract, involving both grey matter and white matter, and to a lesser extent in non-motor regions. More specifically, the results showed significant bilateral atrophy in the motor cortex and corticospinal tract (including the internal capsule and brainstem) and ventricular enlargement, along with significant longitudinal atrophy in precentral gyrus, frontal and parietal white matter, accompanied by ventricular and sulcal enlargement. Atrophy in the precentral gyrus was significantly associated with greater disability as quantified with the Amyotrophic Lateral Sclerosis Functional Rating Scale-Revised ($P < 0.0001$). The pattern of atrophy observed using deformation-based morphometry was consistent with the Brettschneider's four-stage pathological model of the disease. Deformation-based morphometry provides a sensitive indicator of atrophy in Amyotrophic lateral sclerosis and has potential as a biomarker of disease burden, in both grey matter and white matter.

1 Department of Biomedical Engineering, McConnell Brain Imaging Centre, Montreal Neurological Institute, McGill University, Montreal, Quebec H3A 2B4, Canada
2 Sunnybrook Health Sciences Centre, University of Toronto, Toronto, Ontario M4N 3M5, Canada
3 Department of Radiology, Hotchkiss Brain Institute, University of Calgary, Alberta T2N 4N1, Canada
4 Department of Clinical Neurosciences, Hotchkiss Brain Institute, University of Calgary, Alberta T2N 4N1, Canada
5 Seaman Family MR Research Centre, Foothills Medical Centre, Calgary, Alberta T2N 2T9, Canada
6 Montreal Neurological Institute and Hospital, McGill University, Montreal, Quebec H3A 2B4, Canada
7 Neuroscience and Mental Health Institute, University of Alberta, Edmonton, Alberta T6G 2E1, Canada
8 Division of Neurology, Department of Medicine, University of Alberta, Edmonton, Alberta T6G 2R3, Canada

Correspondence to: Mahsa Dadar, PhD McConnell Brain Imaging Centre, Montreal Neurological Institute
McGill University, 3801 University Street, Room WB320, Montréal, Quebec H3A 2B4, Canada
E-mail: mahsa.dadar@mail.mcgill.ca

Keywords: amyotrophic lateral sclerosis; deformation-based morphometry; MRI; mixed-effects modelling

Received February 24, 2020. Revised April 16, 2020. Accepted April 24, 2020. Advance Access publication May 15, 2020

Abbreviations: ALS = amyotrophic lateral sclerosis; ALSFRS-R = ALS Functional Rating Scale-Revised; DBM = deformation-based morphometry; ECAS = Edinburgh Cognitive and Behavioral ALS Screen; FDR = false discovery rate

Graphical Abstract

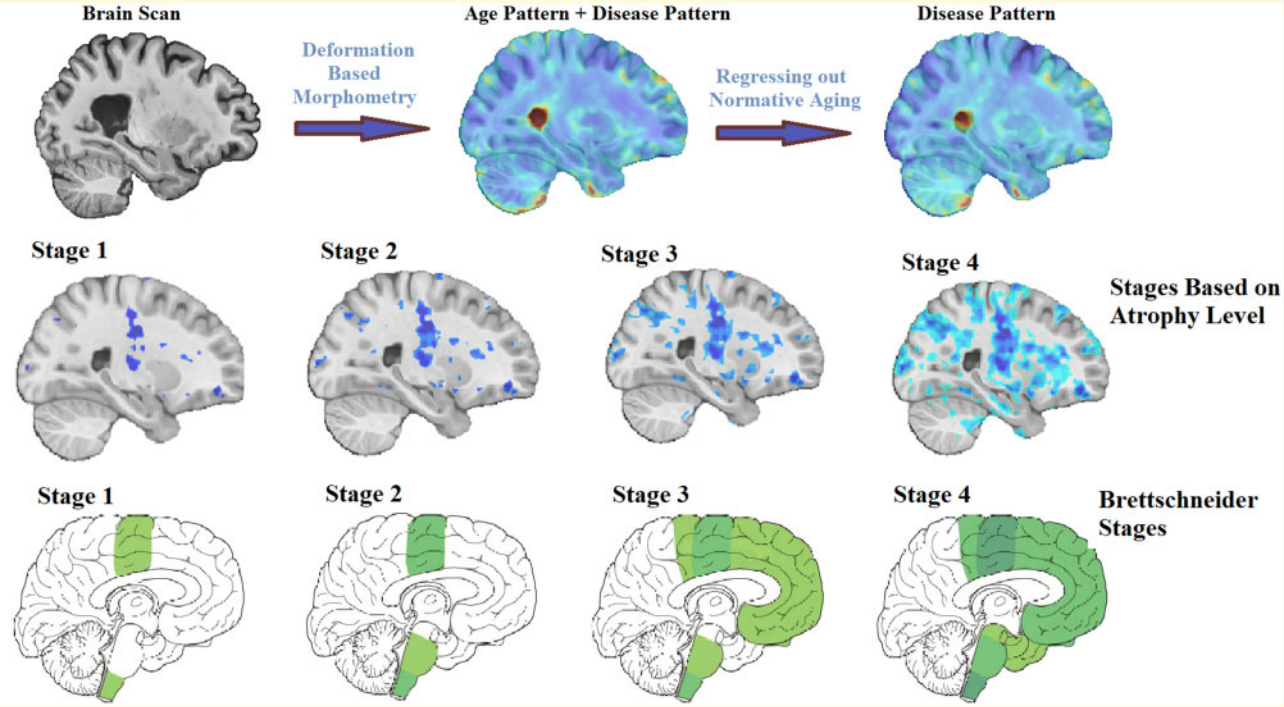

Introduction

Amyotrophic lateral sclerosis (ALS) is a heterogeneous and progressive disorder, characterized by the degeneration of both the upper motor neurons arising from the cortex and lower motor neurons in the brainstem and spinal cord. There is, additionally, extensive involvement of extra-motor regions, including the frontal and temporal lobes (Foerster *et al.*, 2013; Hardiman *et al.*, 2017; Agosta *et al.*, 2018).

The onset of ALS symptoms is variable and can include involvement of limb, bulbar or respiratory muscles or cognitive impairment. Spasticity and hyperreflexia result from upper motor neuron degeneration (Gordon, 2013), whereas fasciculations, cramps and muscle wasting result from lower motor neuron degeneration (Hardiman *et al.*, 2017). Cognitive dysfunction also affects more than half of the patients, with evident frontotemporal dementia in 15% (Wilson *et al.*, 2001; Ringholz *et al.*, 2005). Approximately 30% of all patients have evidence of executive dysfunction at onset, and frontotemporal dementia is one of the presenting features in 13% of incident cases (Hardiman *et al.*, 2017).

Structural MRI studies have demonstrated cross-sectional brain changes in the grey matter and white matter arising from ALS, in both motor and extra-motor areas (Kato *et al.*, 1993; Oba *et al.*, 1993; Waragai, 1997; Andreadou *et al.*, 1998; Hecht *et al.*, 2001; Charil *et al.*, 2009; Foerster *et al.*, 2013; Agosta *et al.*, 2018). Voxel-based morphometry studies report grey matter loss in the motor cortex, as well as in frontotemporal regions especially for patients with cognitive deficits (Chang *et al.*, 2005; Thivard *et al.*, 2007; Agosta *et al.*, 2009*a*, 2007; Senda *et al.*, 2011; Foerster *et al.*, 2013; Sheng *et al.*, 2015; Shen *et al.*, 2016; Buhour *et al.*, 2017; Kim *et al.*, 2017; Agosta *et al.*, 2018; Menke *et al.*, 2018; Chen *et al.*, 2018*b*). Cortical thickness studies have reported cortical thinning in the motor cortex as well as frontal and temporal areas (Roccatagliata *et al.*, 2009; Verstraete *et al.*, 2012; Chen *et al.*, 2018*c*). These studies have generally been performed in relatively small samples of patients and, in particular, longitudinal studies are sparse (Agosta *et al.*, 2009*a*, *b*; Menke *et al.*, 2014, 2018), inherent in this rare and rapidly progressive condition, resulting in challenges with patient recruitment and retention (Foerster *et al.*, 2013; Agosta *et al.*, 2018). Furthermore, insufficient statistical power and differences in image-processing pipelines and statistical analyses have led to variabilities in the reported findings, with studies reporting diverging results such as focal atrophy in

motor/premotor regions, widespread frontotemporal grey matter atrophy sparing the motor cortex or no significant atrophy (Foerster *et al.*, 2013; Agosta *et al.*, 2018).

In this study, we have used deformation-based morphometry (DBM) to quantify the patterns of disease-related brain changes in ALS. DBM allows simultaneous characterization of both mesoscopic and macroscopic changes in brain anatomy in grey matter, white matter and cerebrospinal fluid (Ashburner *et al.*, 1998). In addition, the image-processing tools used in this study have been designed for use in multi-centre datasets across different MRI systems and are able to accommodate between-site variabilities. Taking advantage of these robust methodological tools, our primary goal was to accurately quantify the patterns of disease-related brain changes in ALS and investigate the associations between such changes and clinical symptoms.

In addition, these *in vivo* changes were investigated in relation to the pathological staging system of Brettschneider *et al.* (2013) that characterizes ALS in four stages based on the regional accumulation of transactive response DNA-binding protein 43 kDa. Stage 1 is characterized by the involvement of the primary motor cortex, alpha motor neurons in the ventral horn of the spinal cord and brainstem motor nuclei of cranial nerves V, VII and X–XII. Stage 2 adds involvement of the prefrontal neocortex, reticular formation and the inferior olivary complex. In Stage 3, transactive response DNA-binding protein 43 kDa deposition is now present more extensively in the prefrontal and postcentral neocortex and striatum. Stage 4 additionally involves the anteromedial portions of the temporal lobe, including the hippocampal formation.

We used longitudinal MRI and clinical data from 66 ALS patients and 43 age-matched controls who participated in the Canadian ALS Neuroimaging Consortium to investigate the pattern of brain atrophy in ALS. Three specific hypotheses are addressed: (i) cerebral atrophy is widespread in ALS, involving grey matter, white matter and motor and extra-motor regions; (ii) regional grey and white matter atrophy is correlated with motor and cognitive symptoms; and (iii) the spatial pattern of *in vivo* atrophy aligns with the Brettschneider stages of ALS pathology.

Materials and methods

Participants

Data used in this study included longitudinal (baseline, Month 4 and Month 8) MRI and clinical measurements of 66 ALS patients ($N_{Baseline}$ = 64, N_{Month4} = 44, N_{Month8} = 24) as well as 43 age-matched healthy controls ($N_{Baseline}$ = 42, N_{Month4} = 32, N_{Month8} = 21) from the Canadian ALS Neuroimaging Consortium (http://calsnic.org/, ClinicalTrials.gov NCT02405182). Each participating centre in Canadian ALS Neuroimaging Consortium followed identical standard operating procedures for clinical evaluations and harmonized acquisition protocols for brain imaging. Data from four sites were included: University of Alberta, University of Calgary, University of Toronto and McGill University. All participants gave written informed consent, and the study was approved by the health research ethics boards at each of the participating sites. Participants were included if they had sporadic or familial ALS and met El Escorial criteria for possible, probable, probable laboratory-supported or definite ALS (Brooks *et al.*, 2000). Participants were excluded if they had a history of other neurological or psychiatric disorders, prior brain injury or respiratory impairment resulting in an inability to tolerate the MRI protocol.

Clinical evaluations included global measures of disease status, upper motor neuron dysfunction and cognitive batteries. Disability was assessed with the ALS Functional Rating Scale-Revised (ALSFRS-R), and the annualized disease progression rate was estimated using the formula: (48 − ALSFRS-R)/symptom duration. Finger and foot tapping rates (left and right) were measured and averaged as indicators of upper motor neuron function. Cognitive function was assessed using the Edinburgh Cognitive and Behavioral ALS Screen (ECAS), a multi-domain cognitive screening battery developed for patients with ALS (Abrahams *et al.*, 2014).

The ECAS total score was used to dichotomize patients to impaired versus normal general cognitive status using a cut-off threshold of 2 SDs from the mean of the control subjects. Patients were also dichotomized to impaired versus normal on executive function (ALSexi) based on relevant sub-scores of the ECAS: subjects were considered executively impaired if either the ECAS verbal fluency or ECAS executive score was 2 SDs below the mean of the respective scores in control subjects. Note that the ECAS verbal fluency score is a composite score from two letter fluency tasks and the ECAS executive score is a composite score from tasks of reverse digit span, alternation, sentence completion and social cognition.

All imaging data were acquired on 3 T MRI systems. University of Alberta and McGill University acquired data using Prisma and TimTrio Siemens systems, respectively, and University of Toronto and University of Calgary acquired data using General Electric Healthcare (Discovery MR750) systems. The MRI acquisition protocol included three-dimensional T_1-weighted scans acquired at 1 mm^3 isotropic resolution. Acquisition parameters were identical for the Siemens systems, which used a magnetization prepared rapid gradient echo sequence with repetition time = 2300 ms, echo time = 3.43 ms, inversion time = 900 ms, flip angle = 9°, field of view = 256 mm × 256 mm. The two General Electric systems used identical parameters as well for an inversion recovery-prepared fast spoiled gradient-recalled echo imaging sequence with repetition time = 7.4 ms, echo

time = 3.1 ms, inversion time = 400 ms, flip angle = 11°, field of view = 256 mm × 256 mm.

MRI processing

All T_1-weighted MRI data were pre-processed using the Medical Imaging Network Common dataform toolkit of the Montreal Neurological Institute, publicly available at https://github.com/BIC-MNI/minc-tools, using the following steps: (i) denoising (Coupe *et al.*, 2008); (ii) intensity inhomogeneity correction (Sled *et al.*, 1998); and (iii) image intensity normalization into intensity range (0–100) according to a linear histogram matching algorithm. All images were first linearly (Dadar *et al.*, 2018*a*) and then nonlinearly (Avants *et al.*, 2008) registered to an average template recognized by the International Consortium for Brain Mapping, Montreal Neurological Institute-International Consortium for Brain Mapping 152 (Fonov *et al.*, 2009). The quality of the registrations was visually assessed, confirming that all imaging data were accurately registered to the template.

Using Medical Imaging Network Common tools, DBM maps were obtained by computing the Jacobian of the estimated non-linear deformation field. DBM maps reflect the local differences between the average Montreal Neurological Institute-International Consortium for Brain Mapping 152 template (Fonov *et al.*, 2009) and images of a given participant, with values larger than one indicating expansion (e.g. larger sulci or ventricles) and values smaller than one indicating shrinkage (e.g. atrophy). Voxel-wise DBM maps were used to assess the global brain differences between controls and ALS patients. The mean DBM values across regions of interest were used to assess the relationship between regional atrophy and clinical measurements.

Statistical analyses

To investigate the disease-related cross-sectional and longitudinal changes, normative aging as well as potential sex differences were regressed out from the voxel-wise ALS patient data using the voxel-wise DBM data from the matched controls, as similarly performed in previous studies (La Joie *et al.*, 2012; Moradi *et al.*, 2015; Zeighami *et al.*, 2019; Brown *et al.*, 2019). To achieve this, the following voxel-wise mixed-effects models were estimated based on the controls:

$$\mathrm{DBM} \sim 1 + \mathrm{age} + \mathrm{sex} + (1|\mathrm{ID}) + (1|\mathrm{centre}), \quad (1)$$

where DBM indicates the DBM value at a certain voxel in the brain; age indicates the participant's age at the time of imaging; sex (male/female) is a categorical variable; and ID and centre are categorical random variables, indicating the control participant's ID and the data acquisition centre, respectively. Based on the model estimates, normative aging and sex effects were then regressed out from the patients, yielding residualized DBM values (also known as W-score maps) representing the deviation of the patient measures relative to the value expected in the control group for patient's age and sex (La Joie *et al.*, 2012; Brown *et al.*, 2019). The following mixed-effects models were used to estimate the ALS-specific brain changes in the patients, accounting for confounds:

$$\mathrm{DBMr} \sim 1 + \mathrm{age} + \mathrm{sex} + (1|\mathrm{ID}) + (1|\mathrm{centre}). \quad (2)$$

Here, DBMr are the residualized DBM values [a.k.a. W-score maps, obtained after regressing out age and sex based on controls, i.e. (1)]. The resulting maps were corrected for multiple comparisons using the Benjamini and Hochberg/Yekutieli false discovery rate (FDR) controlling method (Benjamini and Hochberg, 1995; Benjamini and Yekutieli, 2001) with a significance threshold of 0.05.

In addition, the mean DBM values were calculated for the corticospinal tract mask obtained from Yeh *et al.* (2018), as well as the frontal lobe, frontotemporal lobe, precentral gyrus and dorsolateral prefrontal cortex masks obtained from a grey matter atlas for the Montreal Neurological Institute-International Consortium for Brain Mapping 152 template (Manera *et al.*, 2019). The average values were used in the following region-of-interest analyses:

$$\mathrm{DBMr} \sim 1 + \mathrm{clinical\ measure} + (1|\mathrm{ID}) + (1|\mathrm{centre}), \quad (3)$$

where clinical measure indicates either categorical dichotomized scores [e.g. median progression rate (fast/slow)] or continuous values [e.g. ALSFRS-R (0–48)]. The decision on dichotomization of general cognition (ECAS) and executive function (ALSexi) was made due to the fact that the ECAS was performed only at baseline, and therefore, we were not able to measure longitudinal change in these variables. Table 1 indicates the list of the regions and measures of interest tested. The results were corrected for multiple comparisons using the Benjamini and Hochberg/Yekutieli FDR controlling method with a significance threshold of 0.05 (Benjamini and Hochberg, 1995; Benjamini and Yekutieli, 2001). All analyses were performed using MATLAB software (version 2019b). The analyses were performed using 'fitlme' tool, appropriate for performing linear mixed-effects modelling of longitudinal data and accounting for the random effects.

Disease staging based on atrophy

The *t*-statistics W-score map was incrementally thresholded at higher levels to reveal increasing atrophy, starting at −2 (FDR corrected significance level) with one-point increments (i.e. −3, −4 and −5, equivalent to half of the standard deviation from the mean of the *t*-statistics distribution). Four stages with increasing atrophy were identified. The results were then visually compared with the ALS stages defined based on previous pathological staging studies (Brettschneider *et al.*, 2013), based on the regions involved at each stage.

Table 1 Regions and clinical measures of interest assessed in this study

Measure	UMN burden	Progression rate	Cognitive status	Executive impairment	Site of onset	Average tapping rate	ALSFR-S-R
Corticospinal tract	X	X			X	X	X
Precentral gyrus	X	X			X	X	X
Frontotemporal lobe			X				X
Dorsolateral prefrontal cortex				X			

Table 2 Descriptive baseline statistics for the CALSNIC subjects enroled in this study

	Control	ALS	*P*-value
Participants	42	66	
Female	21 (51)	24 (36)	
Age (years)	55.03 ± 8.52 (25–71)	57.98 ± 10.84 (33–80)	0.11
Education (years)	16.12 ± 2.61 (11–28)	14.80 ± 3.26 (4–25)	**0.01**
Symptom duration (years)		3.32 ± 3.03 (0.65–10.91)	
Site of onset (bulbar/limb)		11/52 (17/78%)	
UMN burden (high/low)		20/38 (30/58%)	
Progression rate (high/low)		35/29 (53/44%)	
General cognitive status (impaired/normal on ECAS)		30/33 (46/50%)	
ALSexi: executive impairment (impaired/normal)		26/37 (40/56%)	
Average tapping rate	46.13 ± 12.37 (24.75–67.25)	30.19 ± 15.20 (7–71.75)	<**0.0001**
ALSFRS-R		38.3 ± 5.2 (22–47)	

Data are number of participants in each category (*N*), their percentage of the total population in each category (%), range () and mean ± standard deviation of key demographic variables. Significant differences ($P < 0.05$) are displayed in bold font. Dichotomization details: ECAS: total score, using 2 SD based on controls as cut-off. ALSexi: ECAS Verbal Fluency or ECAS Executive subscore, using 2 SD based on controls as cut-off. UMN burden: above/below (high/low) median value. Progression rate: above/below (high/low) median value. ALSexi = executive impairment; CALSNIC = Canadian ALS Neuroimaging Consortium; UMN = upper motor neuron.

Data availability statement

Anonymized data will be shared at the request of qualified investigators.

Results

Table 2 summarizes the demographic information as well as the clinical scores for the participants used in this study.

Figure 1 shows the *t*-statistics maps reflecting the significant brain volume changes in the ALS cohort, i.e. deviations of the patient DBM measures relative to the value expected in the control group for patient's age and sex, derived from the intercept term in Model 2, after FDR correction. Warm colours indicate areas that are significantly enlarged in the patients in comparison with the controls (e.g. in the sulci and ventricular regions), and cold colours indicate areas of additional shrinkage (i.e. atrophy) in the patients. The results show significant bilateral atrophy in the motor cortex, the corticospinal tract including the internal capsule and brainstem, along with an overall pattern of ventricular enlargement. In addition, significant white matter atrophy was found in anterior cingulate and bilateral posterior parietal areas.

Similarly, Fig. 2 shows the *t*-statistics maps reflecting the significant volume changes with age (derived from the age term in Model 2, after FDR correction) only in the ALS cohort. As normative aging (i.e. the amount of change in the measures estimated based on the control group, i.e. Model 1) has already been regressed out, these remaining changes are the additional ongoing longitudinal changes specific to the disease occurring in the patients. The results show additional atrophy in the precentral gyrus that is more pronounced on the right, as well as diffuse atrophy in frontal and parietal white matter and ventricular and sulcal enlargement.

Table 3 shows the associations between clinical measures and regional atrophy. The mean DBM values in the precentral gyrus were significantly and positively associated with ALSFRS-R, indicating that a lower DBM value (i.e. greater atrophy) related to a lower score in ALSFRS-R (i.e. greater disability). Similarly, the mean DBM value in the corticospinal tract was positively associated with ALSFRS-R, but this relationship did not survive multiple comparison correction (uncorrected *P*-value = 0.03). There was also a trend towards an association between lower mean DBM value in the dorsolateral prefrontal cortex and greater executive impairment (uncorrected *P*-value = 0.08).

Disease staging based on atrophy

t-Statistic thresholds of the W-score map (Fig. 1) at −2, −3, −4 and −5 (FDR corrected and each equivalent to half of the standard deviation from the mean t-statistic distribution) revealed increasing magnitude and spatial extent of atrophy that closely corresponded with the Brettschneider *et al.* (2013) pathological stages (Fig. 3).

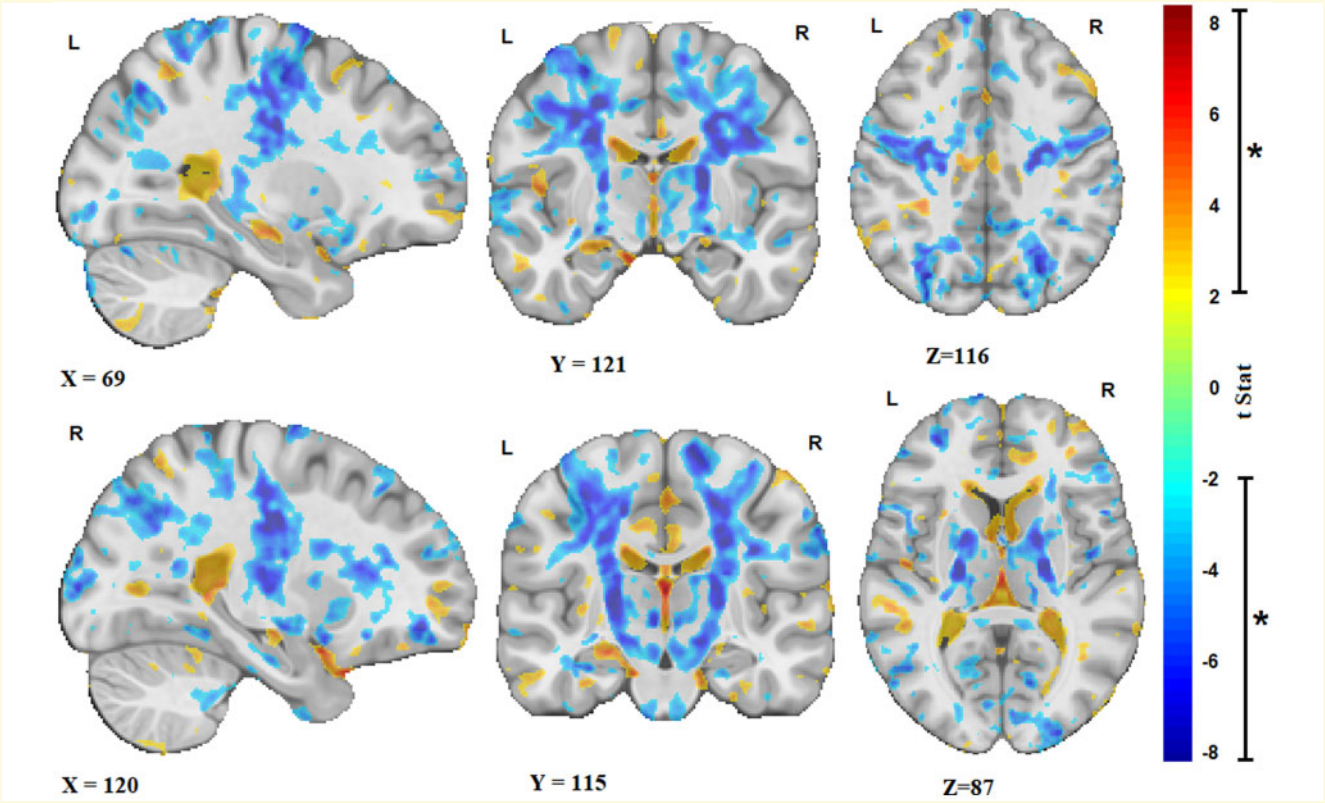

Figure 1 ALS atrophy pattern. Sagittal, coronal and axial slices showing the *t*-statistic maps reflecting the significant patterns of brain volume changes in the ALS cohort [corrected for expected age and sex changes using (1)]. Warm colours indicate enlargement (e.g. ventricular and sulcal regions), and cold colours indicate shrinkage of the tissue (i.e. atrophy). *X*, *Y* and *Z* values indicate MNI coordinates for the displayed slice.

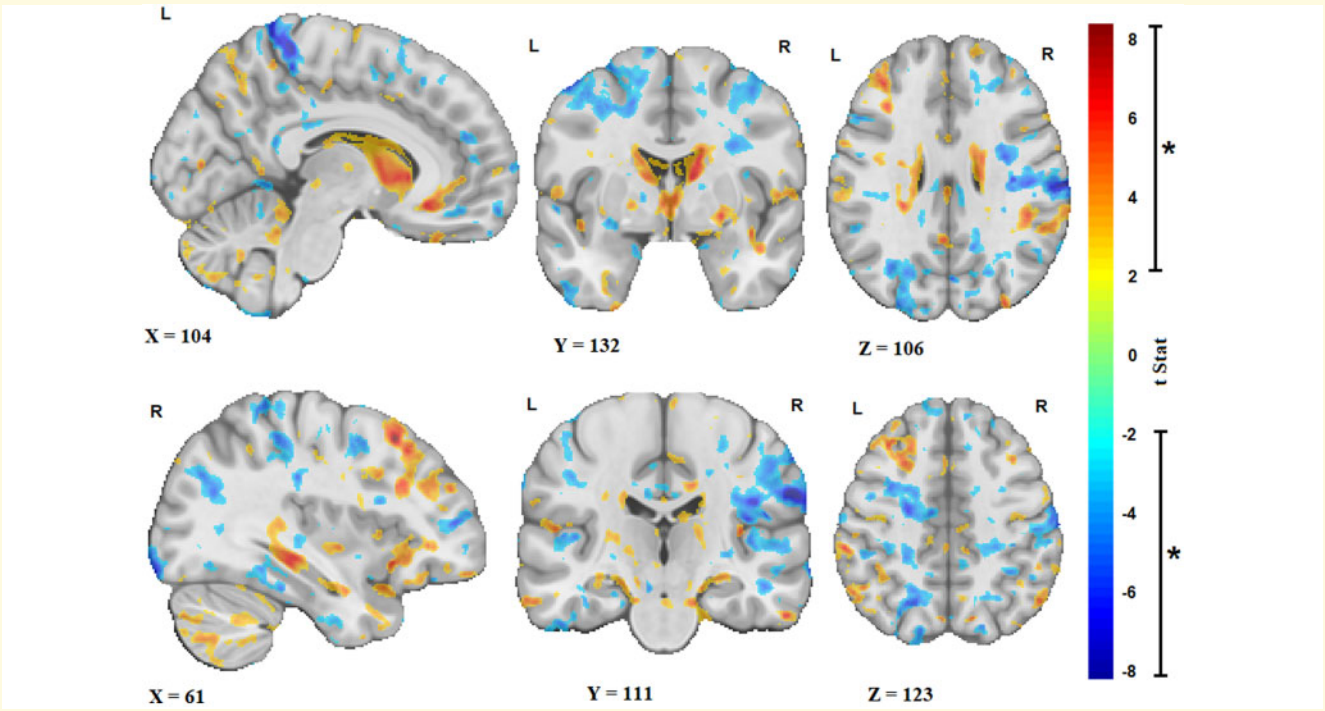

Figure 2 Longitudinal changes. Sagittal, coronal and axial slices showing the *t*-statistic maps reflecting the significant brain volume changes with age (i.e. over time) in the ALS cohort. Warm colours indicate enlargement (e.g. ventricular and sulci regions), and cold colours indicate shrinkage of the tissue (i.e. atrophy). *X*, *Y* and *Z* values indicate MNI coordinates for the displayed slice.

Discussion

The objective of this study was to characterize longitudinal cerebral atrophy in ALS *in vivo*. In line with our hypotheses, it was revealed that atrophy in ALS is extensive, involving bilaterally the motor cortex and corticospinal tracts including the internal capsule and brainstem, and is accompanied by an overall pattern of ventricular enlargement. Longitudinally, atrophy progressed in bilateral precentral gyri, diffuse white matter, and was accompanied by ongoing ventricular and cortical sulcal enlargement. Furthermore, atrophy in the precentral gyrus significantly correlated with disability as assessed with the ALSFRS-R. Finally, the pattern of atrophy is consistent with the pathologically defined stages in ALS by Brettschneider *et al.* (2013). To achieve these results, DBM was applied to T_1-weighted scans from a large multi-centre cohort of ALS from Canadian ALS Neuroimaging Consortium.

Table 3 Summary of the results of the mixed-effects models of associations between regional DBM values and clinical measures

Region	*t*-Statistics	*P*-value
UMN burden		
Corticospinal tract	−0.03	0.97
Precentral gyrus	−0.33	0.74
Progression rate		
Corticospinal tract	1.18	0.24
Precentral gyrus	1.29	0.20
General cognitive status (ECAS)		
Frontotemporal lobe	1.39	0.17
ALSexi		
Dorsolateral prefrontal cortex	−1.72	0.08
Site of onset		
Corticospinal tract	−0.56	0.58
Precentral gyrus	−1.11	0.27
Tapping rate		
Corticospinal tract (contralateral)	0.73	0.46
Precentral gyrus	1.30	0.19
ALSFRS-R		
Corticospinal tract	2.08	0.03
Precentral gyrus	**4.13**	**<0.0001**
Frontotemporal lobe	0.80	0.42

Significant results after correction for multiple comparisons are displayed in bold font.
ALSexi = executive impairment; UMN = upper motor neuron.

Previous imaging studies have reported similar patterns of atrophy. For example, voxel-based morphometry studies have reported gray matter (GM) reduction in motor, premotor, basal ganglia and frontotemporal regions (Chang *et al.*, 2005; Agosta *et al.*, 2007; Thivard *et al.*, 2007; Agosta *et al.*, 2009*a*; Senda *et al.*, 2011; Sheng *et al.*, 2015; Shen *et al.*, 2016; Buhour *et al.*, 2017; Kim *et al.*, 2017; Chen *et al.*, 2018*b*; Menke *et al.*, 2018). A longitudinal tensor-based morphometry study of 16 ALS patients and 10 matched controls (9 months follow-up) found progression of GM atrophy in the left premotor cortex and right basal ganglia in the patients as well as accelerated GM loss in motor and prefrontal areas in patients with faster clinical progression (Agosta *et al.*, 2009*a*). Cortical thickness studies have reported cortical thinning in the motor cortex as well as frontal and temporal areas (Roccatagliata *et al.*, 2009; Verstraete *et al.*, 2012; Chen *et al.*, 2018*c*). A recent meta-analysis

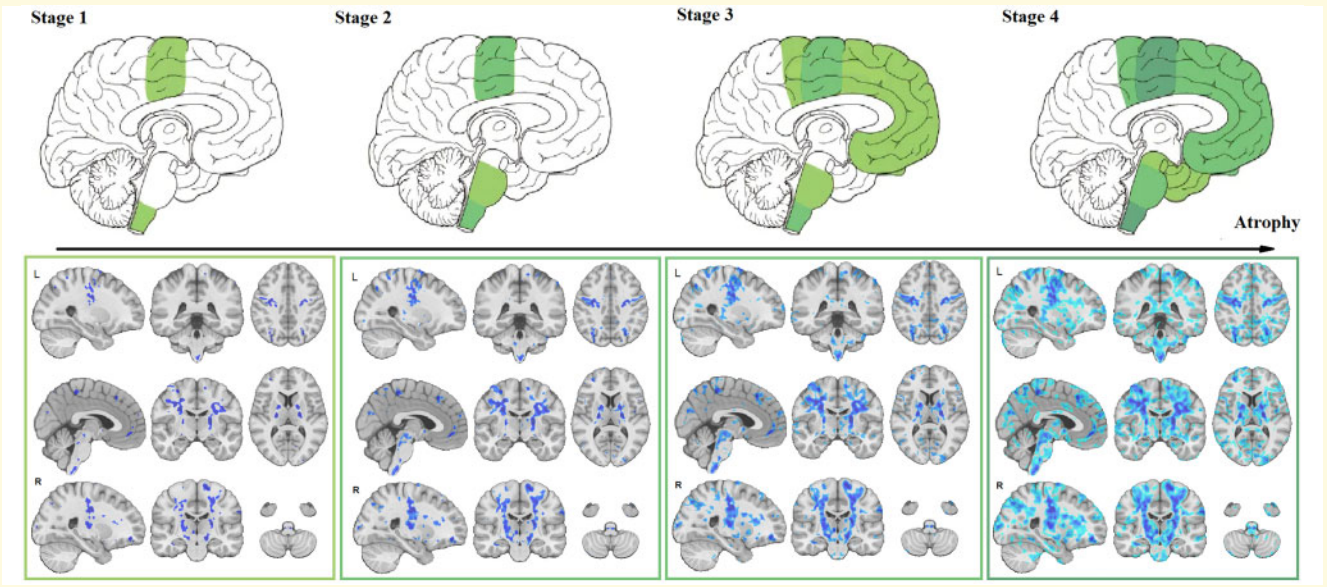

Figure 3 Disease staging. Comparison of disease stages based on the magnitude of atrophy and histological stages. The first row indicates the four pathological stages based on Brettschneider *et al.* (2013) as well as a corresponding sagittal slice from the *t*-statistics map (Fig. 2). The second row shows three sagittal, coronal and axial slices overlayed with the *t*-statistics map values thresholded at *t*-values = −5, −4, −3 and −2, to correspond with Stages 1–4, respectively.

reported significant WM reduction in the bilateral supplementary motor areas, precentral gyri, left middle cerebral peduncle and right cerebellum, involving the corticospinal tract, interhemispheric fibres, subcortical arcuate fibres and the projection fibres to the striatum and cortico-ponto-cerebral tract (Chen *et al.*, 2018*a*).

The atrophy map obtained in this study provides an *in vivo* confirmation for the sequentially increasing pathology in alignment with Brettschneider model (Brettschneider *et al.*, 2013). This sequential pattern of disease progression has also been reported in diffusion tensor imaging studies (Kassubek *et al.*, 2014; Müller *et al.*, 2016; Schmidt *et al.*, 2016). Further studies are necessary to determine the nature of the underlying biological changes (microstructural damage, macrostructural atrophy or a combination) that are observed in T_1-weighted and diffusion tensor imaging (DTI) data. To our knowledge, no previous morphometric study of ALS has succeeded to show the correspondence between the pattern of grey and white matter atrophy and disease stages defined by transactive response DNA-binding protein 43 kDa spreading (Brettschneider *et al.*, 2013). Using different threshold values on the *t*-statistics map (reflecting the severity of atrophy specific to ALS), the four stages described by Brettschneider *et al.* were identified (Fig. 3). The possibility to determine disease stage, and pathological propagation, using structural MRI could have potential implications in the clinical setting. Indeed, using already available and routinely used MRI, non-motor progression of symptoms (i.e. cognitive impairment) could be anticipated. Further studies are necessary to investigate the sensitivity of using structural MRI at the level of an individual participant.

The present study has several advantages compared with the previous reports. The multi-centre Canadian ALS Neuroimaging Consortium cohort included 66 ALS patients, a larger sample size compared with previous studies (Sheng *et al.*, 2015). The MRI scans were also acquired with higher magnetic field strength (i.e. 3 T rather than 1.5 T), yielding images with better contrast. All the image-processing tools used in this study have been developed and extensively validated for use in multi-centre studies involving different MRI systems and have been used in numerous such studies (Zeighami *et al.*, 2015; Dadar *et al.*, 2018*b*; Misquitta *et al.*, 2018; Dadar *et al.*, 2019; Manera *et al.*, 2019; Sanford *et al.*, 2019). In addition, all analyses included 'centre' as a categorical random effect to ensure that any residual variability across centres would not bias the results.

We acknowledge that there were limitations to the present study. Due to the challenges in enrolment and follow-up of the patients in this rare and rapidly progressing disease, the sample sizes of ALS studies (including ours) are in general small compared with other more common neurodegenerative diseases. Attrition is also another common challenge in ALS studies. Not all participants completed all three visits, although the proportion of the number of follow-up visits to baseline was similar across patient and control groups. Furthermore, our follow-up duration was relatively short (8 months). However, since patients with severe symptoms and faster disease progression tend to not complete the follow-up visits, making studies with long follow-up durations biased towards the healthier patients with slower progression rates (Foerster *et al.*, 2013), this relatively short follow-up might have had the advantage of making our findings less biased towards the healthier patients who are more likely to complete longer follow-ups, leading to more generalizable results. Future studies investigating DBM changes in ALS with longer follow-ups are warranted, though there are inherent constraints in recruiting such a cohort.

In conclusion, DBM reveals the atrophy pattern characteristic of ALS consistent with previous pathological findings, both in grey and white matter areas, and can be used to obtain a quantitative measure of disease burden. DBM measurements might therefore have the potential to be a biomarker in ALS.

Funding

The study was funded by the Canadian Institutes of Health Research (CIHR), ALS Canada, and Brain Canada. Data management and quality control were facilitated by the Canadian Neuromuscular Disease Registry.

Competing interests

The authors report no competing interests.

References

Abrahams S, Newton J, Niven E, Foley J, Bak TH. Screening for cognition and behaviour changes in ALS. Amyotroph Lateral Scler Front Degener 2014; 15: 9–14.

Agosta F, Gorno-Tempini ML, Pagani E, Sala S, Caputo D, Perini M, et al. Longitudinal assessment of grey matter contraction in amyotrophic lateral sclerosis: a tensor based morphometry study. Amyotroph Lateral Scler 2009a; 10: 168–74.

Agosta F, Pagani E, Rocca MA, Caputo D, Perini M, Salvi F, et al. Voxel-based morphometry study of brain volumetry and diffusivity in amyotrophic lateral sclerosis patients with mild disability. Hum Brain Mapp 2007; 28: 1430–8.

Agosta F, Rocca MA, Valsasina P, Sala S, Caputo D, Perini M, et al. A longitudinal diffusion tensor MRI study of the cervical cord and brain in amyotrophic lateral sclerosis patients. J Neurol Neurosurg Psychiatry 2009b; 80: 53–5.

Agosta F, Spinelli EG, Filippi M. Neuroimaging in amyotrophic lateral sclerosis: current and emerging uses. Expert Rev Neurother 2018; 18: 395–406.

Andreadou E, Sgouropoulos P, Varelas P, Gouliamos A, Papageorgiou C. Subcortical frontal lesions on MRI in patients with motor neurone disease. Neuroradiology 1998; 40: 298–302.

Ashburner J, Hutton C, Frackowiak R, Johnsrude I, Price C, Friston K. Identifying global anatomical differences: deformation-based morphometry. Hum Brain Mapp 1998; 6: 348–57.

Avants BB, Epstein CL, Grossman M, Gee JC. Symmetric diffeomorphic image registration with cross-correlation: evaluating automated labeling of elderly and neurodegenerative brain. Med Image Anal 2008; 12: 26–41.

Benjamini Y, Hochberg Y. Controlling the false discovery rate: a practical and powerful approach to multiple testing. J R Stat Soc Ser B Methodol 1995; 57: 289–300.

Benjamini Y, Yekutieli D. The control of the false discovery rate in multiple testing under dependency. Ann Stat 2001; 1165–88.

Brettschneider J, Del Tredici K, Toledo JB, Robinson JL, Irwin DJ, Grossman M, et al. Stages of pTDP-43 pathology in amyotrophic lateral sclerosis. Ann Neurol 2013; 74: 20–38.

Brooks BR, Miller RG, Swash M, Munsat TL. El Escorial revisited: revised criteria for the diagnosis of amyotrophic lateral sclerosis. Amyotroph Lateral Scler Other Motor Neuron Disord 2000; 1: 293–9.

Brown J, Deng J, Neuhaus J, Sible IJ, Sias AC, Lee SE, et al. Patient-tailored, connectivity-based forecasts of spreading brain atrophy. Neuron 2019; 104: 856–68.

Buhour M-S, Doidy F, Mondou A, Pélerin A, Carluer L, Eustache F, et al. Voxel-based mapping of grey matter volume and glucose metabolism profiles in amyotrophic lateral sclerosis. EJNMMI Res 2017; 7: 21.

Chang JL, Lomen-Hoerth C, Murphy J, Henry RG, Kramer JH, Miller BL, et al. A voxel-based morphometry study of patterns of brain atrophy in ALS and ALS/FTLD. Neurology 2005; 65: 75–80.

Charil A, Corbo M, Filippi M, Kesavadas C, Agosta F, Munerati E, et al. Structural and metabolic changes in the brain of patients with upper motor neuron disorders: a multiparametric MRI study. Amyotroph Lateral Scler 2009; 10: 269–79.

Chen Z, Liu M, Ma L. Gray matter volume changes over the whole brain in the bulbar- and spinal-onset amyotrophic lateral sclerosis: a voxel-based morphometry study. Chin Med Sci J 2018b; 11: 549–28.

Chen Z, Liu M, Ma L. Cortical thinning pattern of bulbar- and spinal-onset amyotrophic lateral sclerosis: a surface-based morphometry study. Chin Med Sci J 2018c; 33: 100–6.

Chen G, Zhou B, Zhu H, Kuang W, Bi F, Ai H, et al. White matter volume loss in amyotrophic lateral sclerosis: a meta-analysis of voxel-based morphometry studies. Prog Neuropsychopharmacol Biol Psychiatry 2018a; 83: 110–7.

Coupe P, Yger P, Prima S, Hellier P, Kervrann C, Barillot C. An optimized blockwise nonlocal means denoising filter for 3-D magnetic resonance images. IEEE Trans Med Imaging 2008; 27: 425–41.

Dadar M, Fonov VS, Collins DL, Initiative A. A comparison of publicly available linear MRI stereotaxic registration techniques. Neuroimage 2018a; 174: 191–200.

Dadar M, Maranzano J, Ducharme S, Collins DL. White matter in different regions evolves differently during progression to dementia. Neurobiol Aging 2019; 76: 71–9.

Dadar M, Zeighami Y, Yau Y, Fereshtehnejad S-M, Maranzano J, Postuma RB, et al. White matter hyperintensities are linked to future cognitive decline in de novo Parkinson's disease patients. Neuroimage Clin 2018b; 20: 892–900.

Foerster BR, Welsh RC, Feldman EL. 25 years of neuroimaging in amyotrophic lateral sclerosis. Nat Rev Neurol 2013; 9: 513–24.

Fonov V, Evans A, McKinstry R, Almli C, Collins D. Unbiased nonlinear average age-appropriate brain templates from birth to adulthood. Neuroimage 2009; 47: S102.

Gordon PH, Amyotrophic lateral sclerosis: an update for 2013 clinical features, pathophysiology, management and therapeutic trials. Aging Dis 2013; 04: 295–310.

Hardiman O, Al-Chalabi A, Chio A, Corr EM, Logroscino G, Robberecht W, et al. Amyotrophic lateral sclerosis. Nat Rev Dis Primer 2017; 3: 17071.

Hecht MJ, Fellner F, Fellner C, Hilz MJ, Heuss D, Neundörfer B. MRI-FLAIR images of the head show corticospinal tract alterations in ALS patients more frequently than T2-, T1-and proton-density-weighted images. J Neurol Sci 2001; 186: 37–44.

Kassubek J, Müller H-P, Del Tredici K, Brettschneider J, Pinkhardt EH, Lule D, et al. Diffusion tensor imaging analysis of sequential spreading of disease in amyotrophic lateral sclerosis confirms patterns of TDP-43 pathology. Brain 2014; 137: 1733–40.

Kato S, Hayashi H, Yagishita A. Involvement of the frontotemporal lobe and limbic system in amyotrophic lateral sclerosis: as assessed by serial computed tomography and magnetic resonance imaging. J Neurol Sci 1993; 116: 52–8.

Kim H-J, Leon M, de Wang X, Kim HY, Lee Y-J, Kim Y-H, et al. Relationship between clinical parameters and brain structure in sporadic amyotrophic lateral sclerosis patients according to onset type: a voxel-based morphometric study. PLoS One 2017; 12: e0168424.

La Joie R, Perrotin A, Barré L, Hommet C, Mézenge F, Ibazizene M, et al. Region-specific hierarchy between atrophy, hypometabolism, and β-amyloid (Aβ) load in Alzheimer's disease dementia. J Neurosci 2012; 32: 16265–73.

Manera AL, Dadar M, Collins DL, Ducharme S, Initiative F. Deformation based morphometry study of longitudinal MRI changes in behavioral variant frontotemporal dementia. Neuroimage Clin 2019; 24: 102079.

Menke RAL, Körner S, Filippini N, Douaud G, Knight S, Talbot K, et al. Widespread grey matter pathology dominates the longitudinal cerebral MRI and clinical landscape of amyotrophic lateral sclerosis. Brain 2014; 137: 2546–55.

Menke RAL, Proudfoot M, Talbot K, Turner MR. The two-year progression of structural and functional cerebral MRI in amyotrophic lateral sclerosis. Neuroimage Clin 2018; 17: 953–61.

Misquitta K, Dadar M, Tarazi A, Hussain MW, Alatwi MK, Ebraheem A, et al. The relationship between brain atrophy and cognitive-behavioural symptoms in retired Canadian football players with multiple concussions. Neuroimage Clin 2018; 19: 551–8.

Moradi E, Pepe A, Gaser C, Huttunen H, Tohka J, Initiative ADN, et al. Machine learning framework for early MRI-based Alzheimer's conversion prediction in MCI subjects. Neuroimage 2015; 104: 398–412.

Müller H-P, Turner MR, Grosskreutz J, Abrahams S, Bede P, Govind V, et al. A large-scale multicentre cerebral diffusion tensor imaging study in amyotrophic lateral sclerosis. J Neurol Neurosurg Psychiatry 2016; 87: 570–9.

Oba H, Araki T, Ohtomo K, Monzawa S, Uchiyama G, Koizumi K, et al. Amyotrophic lateral sclerosis: T2 shortening in motor cortex at MR imaging. Radiology 1993; 189: 843–6.

Ringholz GM, Appel SH, Bradshaw M, Cooke NA, Mosnik DM, Schulz PE. Prevalence and patterns of cognitive impairment in sporadic ALS. Neurology 2005; 65: 586–90.

Roccatagliata L, Bonzano L, Mancardi G, Canepa C, Caponnetto C. Detection of motor cortex thinning and corticospinal tract involvement by quantitative MRI in amyotrophic lateral sclerosis. Amyotroph Lateral Scler 2009; 10: 47–52.

Sanford R, Strain J, Dadar M, Maranzano J, Bonnet A, Mayo NE, et al. HIV infection and cerebral small vessel disease are independently associated with brain atrophy and cognitive impairment. AIDS 2019; 33: 1197–205.

Schmidt R, de Reus MA, Scholtens LH, van den Berg LH, van den Heuvel MP. Simulating disease propagation across white matter connectome reveals anatomical substrate for neuropathology staging in amyotrophic lateral sclerosis. Neuroimage 2016; 124: 762–9.

Senda J, Kato S, Kaga T, Ito M, Atsuta N, Nakamura T, et al. Progressive and widespread brain damage in ALS: MRI voxel-based morphometry and diffusion tensor imaging study. Amyotroph Lateral Scler 2011; 12: 59–69.

Shen D, Cui L, Fang J, Cui B, Li D, Tai H. Voxel-wise meta-analysis of gray matter changes in amyotrophic lateral sclerosis. Front Aging Neurosci 2016; 8: 64.

Sheng L, Ma H, Zhong J, Shang H, Shi H, Pan P. Motor and extra-motor gray matter atrophy in amyotrophic lateral sclerosis: quantitative meta-analyses of voxel-based morphometry studies. Neurobiol Aging 2015; 36: 3288–99.

Sled JG, Zijdenbos AP, Evans AC. A nonparametric method for automatic correction of intensity nonuniformity in MRI data. IEEE Trans Med Imaging 1998; 17: 87–97.

Thivard L, Pradat P-F, Lehéricy S, Lacomblez L, Dormont D, Chiras J, et al. Diffusion tensor imaging and voxel based morphometry study in amyotrophic lateral sclerosis: relationships with motor disability. J Neurol Neurosurg Psychiatry 2007; 78: 889–92.

Verstraete E, Veldink JH, Hendrikse J, Schelhaas HJ, van den Heuvel MP, van den Berg LH. Structural MRI reveals cortical thinning in amyotrophic lateral sclerosis. J Neurol Neurosurg Psychiatry 2012; 83: 383–8.

Waragai M. MRI and clinical features in amyotrophic lateral sclerosis. Neuroradiology 1997; 39: 847–51.

Wilson CM, Grace GM, Munoz DG, He BP, Strong MJ. Cognitive impairment in sporadic ALS: a pathologic continuum underlying a multisystem disorder. Neurology 2001; 57: 651–7.

Yeh F-C, Panesar S, Fernandes D, Meola A, Yoshino M, Fernandez-Miranda JC, et al. Population-averaged atlas of the macroscale human structural connectome and its network topology. Neuroimage 2018; 178: 57–68.

Zeighami Y, Fereshtehnejad S-M, Dadar M, Collins DL, Postuma RB, Miić B, et al. A clinical-anatomical signature of Parkinson's Disease identified with partial least squares and magnetic resonance imaging. Neuroimage 2019; 190: 69–78.

Zeighami Y, Ulla M, Iturria-Medina Y, Dadar M, Zhang Y, Larcher K-H, et al. Network structure of brain atrophy in de novo Parkinson's disease. eLife 2015; 4: e08440.